

# Translational and rotational near-wall diffusion of spherical colloids studied by evanescent wave scattering

Cite this: *Soft Matter*, 2014, 10, 4312

Maciej Lisicki,<sup>\*a</sup> Bogdan Cichocki,<sup>a</sup> Simon A. Rogers,<sup>b</sup> Jan K. G. Dhont<sup>cd</sup> and Peter R. Lang<sup>c</sup>

In this article we extend recent experimental developments [Rogers *et al.*, *Phys. Rev. Lett.*, 2012, 109, 098305] by providing a suitable theoretical framework for the derivation of exact expressions for the first cumulant (initial decay rate) of the correlation function measured in Evanescent Wave Dynamic Light Scattering (EWDLS) experiments. We focus on a dilute suspension of optically anisotropic spherical Brownian particles diffusing near a planar hard wall. In such a system, translational and rotational diffusion are hindered by hydrodynamic interactions with the boundary which reflects the flow incident upon it, affecting the motion of colloids. The validity of the approximation by the first cumulant for moderate times is assessed by juxtaposition to Brownian dynamics simulations, and compared with experimental results. The presented method for the analysis of experimental data allows the determination of penetration-depth-averaged rotational diffusion coefficients of spherical colloids at low density.

Received 7th January 2014

Accepted 9th April 2014

DOI: 10.1039/c4sm00148f

www.rsc.org/softmatter

## 1 Introduction

Rotational diffusion plays a crucial role in a number of physical, chemical, and biological processes occurring in a variety of systems. Notable examples include microrheology, in which frequency-dependent viscoelastic shear moduli can be investigated by measuring rotational diffusion of a tracer sphere;<sup>1</sup> random reorientation of biomacromolecules in membranes (like proteins in human erythrocyte membrane,<sup>2</sup> or rhodopsin chromophores<sup>3</sup>); rotational-diffusion controlled chemical reactivity;<sup>4–6</sup> and gaseous combustion models, where rotational diffusion is of importance for the interpretation of coherent anti-Stokes Raman spectroscopy data.<sup>7</sup> Much attention has been devoted over the last decade to rotational diffusion of bulk systems, particularly in the context of macromolecules. Similar systems in geometrical confinement are, however, much less understood, and are becoming a very active field of research. This is motivated by the fundamental importance of the effects of confinement for macromolecular solutions, which are most pronounced in the small-scale channel flows which are an inherent feature of micro-<sup>8</sup> nano-<sup>9</sup> and optofluidics.<sup>10</sup> An

illustrative example may be given in the rapidly growing “lab-on-a-chip” applications, in which a single colloid might be used as a micropump,<sup>11</sup> or by investigation of swimming microorganisms,<sup>12</sup> nutrition of which is strongly influenced by their hydrodynamic interactions;<sup>13</sup> confined geometry plays a key role also in chip-based capillary electrophoresis<sup>14</sup> and sorting of white blood cells.<sup>4</sup>

To investigate the effects of confinement on rotational diffusion of Brownian particles, we have employed Evanescent Wave Dynamic Light Scattering<sup>15</sup> (EWDLS), which is a technique that probes the near-wall dynamics of submicron-sized particles. In the experiments, only the region of the sample close to the boundary is illuminated, as the electric field strength of an evanescent wave decays with distance  $z$  away from the wall as  $\exp(-\kappa z/2)$ . The characteristic length scale  $2/\kappa$ , called the penetration depth, is typically of the order of several hundred nanometers. Using this feature, one can infer information on the effects of hydrodynamic interactions with the surface on the dynamics of suspended colloids. By changing the scattering vector  $q$ , the system is probed on different length scales.

Starting with the pioneering work by Lan and Ostrowsky,<sup>15</sup> EWDLS has been employed frequently to investigate the near surface dynamics of soft matter. The translational diffusion of colloids has been studied in dilute solutions<sup>16–18</sup> and in suspensions with volume fractions up to 45 percent.<sup>19,20,21</sup> The dynamics of stiff polymers adsorbed to the interface<sup>22</sup> were investigated as well as the collective motion of end-grafted polymer brushes.<sup>23,24</sup> With a setup that allows independent

<sup>a</sup>Institute of Theoretical Physics, Faculty of Physics, University of Warsaw, ul. Hoża 69, 00-681 Warsaw, Poland. E-mail: mklis@fuw.edu.pl

<sup>b</sup>Department of Chemical and Biomolecular Engineering, University of Delaware, Newark, DE 19716, USA

<sup>c</sup>ICS-3, Institute of Complex Systems, Forschungszentrum Jülich, D-52425 Jülich, Germany

<sup>d</sup>Heinrich-Heine University, Department of Physics, Düsseldorf, Germany

variation of the components of the scattering vector  $q_{\parallel}$ ,  $q_{\perp}$ , parallel and perpendicular to the surface, respectively, it is possible to distinguish between the diffusivities of colloidal particles in these directions experimentally.<sup>25,26</sup>

In recent contributions,<sup>27,28</sup> we have presented a study of applicability of EWDLS to trace translational, as well as rotational diffusion in dilute suspensions in which single-particle properties completely characterise the system. By means of cumulant expansion based on the Smoluchowski equation, we have developed exact expressions for the initial decay rate of the electric field time autocorrelation function, which is related to the experimentally determined intensity time autocorrelation function by a generalized Siegert relation.<sup>26</sup> In case of purely translational motion,<sup>27</sup> terms up to quadratic order in time have been shown to describe the decay of the correlation function up to moderate times. Comparison with experiments and Brownian dynamics simulations resulted in fair agreement of the data. Using optically anisotropic spheres,<sup>28</sup> we were able to record orientation-dependent signal in the correlation function and extract from experiments the rotational diffusion coefficients which proved to be consistent with theoretical calculations.<sup>29</sup> Rotational diffusion of spherical particles measured by light scattering has been extensively studied in bulk, both theoretically,<sup>30</sup> and experimentally using systems of optically anisotropic spherical Brownian particles.<sup>31–33</sup> It seems, however, that apart from theoretical and numerical calculations for rotational diffusion of spheres confined to diffuse near a wall,<sup>29,34–38</sup> or in a parallel-wall channel,<sup>39</sup> there has been no experimental investigation of rotational diffusion in such confined systems, and our research aims to fill this gap using a recently developed experimental technique followed by a thorough analysis of its theoretical basis.

In this work, we present a detailed derivation of the first cumulant for translational, rotational, and coupled motion of a Brownian sphere above a solid hard wall, extending the analysis from our previous article<sup>28</sup> where only the final experimental results were published. Theoretical developments are followed by results of experiments, and numerical simulations.

The paper is organised as follows: in Section 2 we describe the system and the basic quantities measured in the experiments. Next, in Section 3, we introduce the Smoluchowski equation and discuss the hydrodynamic interactions between a spherical particle and a planar wall. This description is then used in Section 4 to derive analytical expressions for the first cumulant, which describes the short-time decay of the measured electric field correlation functions. In Section 5, we go beyond the short time limit by means of a Brownian dynamics simulation. The experimental details are included in Section 6. Section 7 contains the results of experiments compared to numerical calculations and theoretical predictions. Finally, we conclude our findings in Section 8. Two appendices contain a proof of vanishing translation–rotation coupling contribution to the first cumulant, and the details of our numerical code, respectively.

## 2 Intensity correlation function in evanescent wave dynamic light scattering

In EWDLS experiments, as well as in any conventional light scattering experimental technique, one measures the scattered light intensity time autocorrelation function  $g_2(\mathbf{q}, t)$ , defined as

$$g_2(\mathbf{q}, t) = \frac{\langle I_s(\mathbf{q}, t=0)I_s(\mathbf{q}, t) \rangle}{\langle I_s(\mathbf{q}, t=0) \rangle^2}, \quad (1)$$

where  $I_s(\mathbf{q}, t)$  is the intensity of light scattered at time  $t$  in the direction given by the scattering vector  $\mathbf{q}$ . Here  $\langle \dots \rangle$  denotes the equilibrium ensemble averaging. The scattered intensity is related to the corresponding electric field,  $E_s$ , through  $I_s(\mathbf{q}, t) = |E_s(\mathbf{q}, t)|^2$ . By virtue of the Siegert relation,<sup>40</sup> the function  $g_2(\mathbf{q}, t)$  may be written in terms of the scattered electric field autocorrelation function

$$g_1(\mathbf{q}, t) = \frac{\langle E_s^*(\mathbf{q}, t=0)E_s(\mathbf{q}, t) \rangle}{\langle |E_s(\mathbf{q}, t=0)|^2 \rangle}. \quad (2)$$

For purely homodyne detection, the Siegert relation has the form

$$g_2(\mathbf{q}, t) = 1 + |g_1(\mathbf{q}, t)|^2. \quad (3)$$

The above relation has also been generalised to mixed homodyne and heterodyne detection.<sup>25,26</sup> The field autocorrelation function  $g_1(\mathbf{q}, t)$  will be the main object of our interest.

In a wall-bounded system, the suspension is illuminated by an evanescent wave, in which the electric field decays exponentially with distance from the boundary. Since we are interested in the dilute limit, we restrict to single-particle quantities, as we described in detail in earlier works.<sup>27</sup> The scattered electric field has the form

$$E_s(\mathbf{q}, t) \sim \mathcal{E}(\hat{\mathbf{u}})\exp\{i\mathbf{q}\cdot\mathbf{r}(t)\}\exp\left\{-\frac{\kappa}{2}z(t)\right\}, \quad (4)$$

where  $\mathbf{r}$  is the position of the particle at a distance  $z$  from the wall, having the orientation  $\hat{\mathbf{u}}$ . The orientation-dependent part  $\mathcal{E}(\hat{\mathbf{u}})$  is the oriented dielectric tensor of the particle<sup>41</sup>

$$\mathcal{E}(\hat{\mathbf{u}}) = \hat{\mathbf{n}}_s \cdot \boldsymbol{\varepsilon}(\hat{\mathbf{u}}) \cdot \hat{\mathbf{n}}_0, \quad (5)$$

where  $\hat{\mathbf{n}}_0$  and  $\hat{\mathbf{n}}_s$  are the polarisation directions of the incident and scattered light, respectively. Since we are interested in the dynamics of a spherical colloidal particle, the only anisotropy comes from its optical properties. The latter may be described by introducing the dielectric tensor of the particle<sup>41</sup>

$$\boldsymbol{\varepsilon}(\hat{\mathbf{u}}) = \alpha \mathbf{1} + \Delta\alpha \left( \hat{\mathbf{u}}\hat{\mathbf{u}} - \frac{1}{3}\mathbf{1} \right), \quad (6)$$

with  $\alpha$  and  $\Delta\alpha$  being the complex mean polarisability and polarisation anisotropy of the particle, respectively. They are related to particle polarisabilities  $\alpha_{\parallel, \perp}$  in directions parallel and perpendicular to its axis  $\hat{\mathbf{u}}$  by

$$\alpha = \frac{1}{3}(\alpha_{\parallel} + 2\alpha_{\perp}), \Delta\alpha = \alpha_{\parallel} - \alpha_{\perp}. \quad (7)$$

The electric field autocorrelation function is often analysed by means of its initial decay rate, called the first cumulant

$$\Gamma = -\lim_{t \rightarrow 0} \frac{\partial g_1(\mathbf{q}, t)}{\partial t}. \quad (8)$$

In the course of this paper, we shall derive exact expressions for the first cumulant in the case of a dilute suspension of optically anisotropic spheres.

We first note, however, that in the limit of infinitely large penetration depth, corresponding to  $\kappa \rightarrow 0$ , eqn (4) simplifies, and we recover bulk results, known from standard depolarised dynamic light scattering (DDLS). In this case, the decay of  $g_1(\mathbf{q}, t)$  for a dilute suspension of spherical particles is strictly exponential in time

$$g_1(\mathbf{q}, t) = \exp(-\Gamma_0 t). \quad (9)$$

The first cumulant contains both rotational and translational contributions

$$\Gamma_0 = \Gamma_0^t + \Gamma_0^r. \quad (10)$$

The rotational part depends on the polarisation of the incident and scattered light beam, encoded in unit vectors  $\hat{\mathbf{n}}_0$  and  $\hat{\mathbf{n}}_s$ . If we set the polarisation direction of the incident beam to be  $\hat{\mathbf{n}}_0 = (1, 0, 0)$ , we may distinguish two cases: (i)  $\hat{\mathbf{n}}_s = \hat{\mathbf{n}}_0$ , referred to as VV-geometry, and (ii)  $\hat{\mathbf{n}}_0 \cdot \hat{\mathbf{n}}_s = 0$ , called the VH-geometry. In this case  $\hat{\mathbf{n}}_s = (0, n_y, n_z)$  and since it is a unit vector  $n_y^2 + n_z^2 = 1$ . In this notation the  $x$ -direction is normal to the plane spanned by the wave vector of the scattered  $\mathbf{k}_s$  and that of the incident light  $\mathbf{k}_i$  while the  $y$ -direction is parallel to  $\mathbf{k}_i$ .

The first cumulant in bulk has then the following parts, given by Berne and Pecora<sup>41†</sup>

$$\Gamma_0^t = q^2 D_0^t, \quad (11)$$

$$\text{VH: } \Gamma_0^r = 6D_0^r, \quad (12)$$

$$\text{VV: } \Gamma_0^r = \frac{24|\Delta\alpha|^2}{45|\alpha|^2 + 4|\Delta\alpha|^2} D_0^r. \quad (13)$$

Here, the bulk diffusion coefficients for a sphere in an infinite fluid are given by

$$D_0^t = \frac{k_B T}{6\pi\eta a}, D_0^r = \frac{k_B T}{8\pi\eta a^3}, \quad (14)$$

where  $k_B$  is the Boltzmann constant,  $T$  is the temperature,  $a$  is the particle radius, and  $\eta$  is the viscosity of the solvent.

† In Section 7.3 of the book by Berne and Pecora,<sup>41</sup> only the full expressions for the translational and rotational parts of  $g_1(\mathbf{q}, t)$  in bulk are given. To arrive at eqn (11)–(13), one has to calculate their derivatives at  $t = 0$ , in accordance with eqn (8).

We would like to stress that there are two essential differences between a bulk DDLS experiment and an EWDLS measurement. Firstly, in an evanescent field the illumination intensity varies on the length scales of the penetration depth  $2/\kappa$ , comparable to the size of particles. In the presence of an evanescent wave, the strength of the electric field incident on the particle decreases exponentially with its distance from the wall. Hence only the particles staying within distances of the order of the penetration depth from the wall scatter enough light to be detected. Secondly, since the boundary of the system reflects the flow caused by motion of the particles, affecting their motion in return, the hydrodynamic mobility of particles becomes dependent on their distance from the wall. This fact, which we will discuss in detail in the next section, has a major impact on the dynamics of the system. The interplay between non-uniform illumination and hydrodynamic effects renders the interpretation of measurements much more involved.

### 3 Near-wall diffusion of a spherical particle – theoretical description

We consider a dilute suspension of spherical Brownian particles of radius  $a$  bounded by a hard wall at  $z = 0$  (see Fig. 1). In this case, the problem reduces to a single-particle one, and the system may be described in terms of the probability distribution  $P(\mathbf{X}, t)$  of finding the particle in configuration  $\mathbf{X}$  at time  $t$ , with  $\mathbf{X} = (\mathbf{r}, \hat{\mathbf{u}})$ , where  $\mathbf{r}$  is its position vector, and  $\hat{\mathbf{u}}$  is a unit vector specifying the orientation of the particle, which is given by its main optical axis, in accordance with eqn (6). The normalisation reads

$$\int d\mathbf{X} P(\mathbf{X}, t) = 1, \quad (15)$$

where  $d\mathbf{X} = d\mathbf{r}d\hat{\mathbf{u}}$ . The integral over  $\mathbf{X}$  is taken with respect to the position of the particle  $\mathbf{r}$  over the wall-bounded half-space, and to its orientation  $\hat{\mathbf{u}}$  over a spherical unit surface. This probability density obeys the Smoluchowski equation of the form<sup>42</sup>

$$\frac{\partial}{\partial t} P(\mathbf{X}, t) = \mathcal{L}P(\mathbf{X}, t). \quad (16)$$

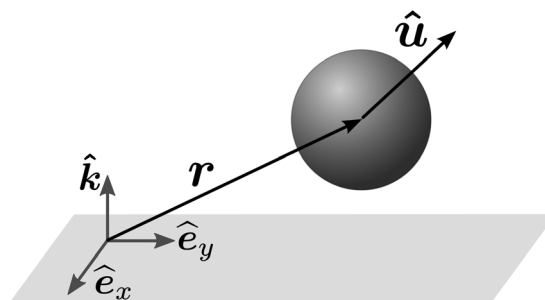


Fig. 1 The geometry of the system. A single particle, placed in  $\mathbf{r}$  and having the orientation  $\hat{\mathbf{u}}$ , diffuses near a planar hard wall at  $z = 0$ . The  $z$ -direction is given by a unit vector  $\hat{\mathbf{k}} \equiv \hat{\mathbf{e}}_z$ .

The Smoluchowski evolution operator  $\mathcal{L}$  may be written as

$$\mathcal{L}P = \nabla_X \cdot \mathbf{D} \cdot [\beta P (\nabla_X \Phi) + \nabla_X P], \quad (17)$$

where  $\beta = 1/k_B T$ , and  $\mathbf{D}$  is the  $6 \times 6$  diffusion matrix. The gradient operator is defined as

$$\nabla_X = \left( \frac{\partial}{\partial \mathbf{r}}, \mathbf{L} \right). \quad (18)$$

The rotational operator may be written in terms of the particle orientation as<sup>42</sup>

$$\mathbf{L} = \hat{\mathbf{u}} \times \frac{\partial}{\partial \hat{\mathbf{u}}}, \quad (19)$$

where  $\frac{\partial}{\partial \hat{\mathbf{u}}}$  is the gradient operator with respect to the Cartesian coordinates of  $\hat{\mathbf{u}}$ . Finally, the  $6 \times 6$  diffusion matrix  $\mathbf{D}$  can be related to the particle mobility matrix  $\boldsymbol{\mu}$  by the fluctuation-dissipation relation

$$\mathbf{D} = k_B T \boldsymbol{\mu}. \quad (20)$$

The mobility matrix  $\boldsymbol{\mu}$  relates the force  $\mathbf{F}$  and torque  $\mathbf{T}$  exerted on the particle to its linear and angular velocities,  $\mathbf{U}$  and  $\boldsymbol{\Omega}$ , as

$$\begin{pmatrix} \mathbf{U} \\ \boldsymbol{\Omega} \end{pmatrix} = \boldsymbol{\mu} \cdot \begin{pmatrix} \mathbf{F} \\ \mathbf{T} \end{pmatrix}. \quad (21)$$

The mobility matrix  $\boldsymbol{\mu}$  consists of four  $3 \times 3$  submatrices,

$$\boldsymbol{\mu} = \begin{pmatrix} \boldsymbol{\mu}^{tt} & \boldsymbol{\mu}^{tr} \\ \boldsymbol{\mu}^{rt} & \boldsymbol{\mu}^{rr} \end{pmatrix}, \quad (22)$$

where the indices tt and rr denote the translational and rotational parts, respectively. The tr and rt matrices describe the coupling between translational and rotational motion.

For an unbounded suspension, the diffusion tensors become proportional to the isotropic unit tensor  $\mathbf{1}$

$$\mathbf{D}_0^t = D_0^t \mathbf{1}, \quad \mathbf{D}_0^r = D_0^r \mathbf{1}, \quad (23)$$

and the tr and rt coupling tensors vanish.

In the wall-bounded system, due to hydrodynamic interactions with the wall, all the diffusion coefficients depend on the wall-particle distance  $z$ . However, due to the spherical shape of the particle, its hydrodynamic properties are independent of the orientation. From the symmetries of the system, one concludes that the translational and rotational diffusion tensors have the following structure

$$\mathbf{D}^{tt} = D_{\perp}^t(z) \hat{\mathbf{k}} \hat{\mathbf{k}} + D_{\parallel}^t(z) (\mathbf{1} - \hat{\mathbf{k}} \hat{\mathbf{k}}), \quad (24)$$

$$\mathbf{D}^{rr} = D_{\perp}^r(z) \hat{\mathbf{k}} \hat{\mathbf{k}} + D_{\parallel}^r(z) (\mathbf{1} - \hat{\mathbf{k}} \hat{\mathbf{k}}), \quad (25)$$

$$\mathbf{D}^{tr} = D^{tr}(z) \boldsymbol{\varepsilon} \cdot \hat{\mathbf{k}}, \quad (26)$$

$$\mathbf{D}^{rt} = D^{rt}(z) \boldsymbol{\varepsilon} \cdot \hat{\mathbf{k}}, \quad (27)$$

where  $\hat{\mathbf{k}}$  is a unit vector normal to the wall, pointing into the fluid,  $\mathbf{1}$  is the identity matrix, and  $\boldsymbol{\varepsilon}$  is the Levi-Civita tensor.

In addition, the translational-rotational parts obey the relation

$$\mathbf{D}^{tr} = (\mathbf{D}^{rt})^T, \quad (28)$$

where T denotes transposition. Hence we conclude that  $\mathbf{D}^{tr} = -\mathbf{D}^{rt}$ . With all the symmetries described above, we have written the Smoluchowski equation for this case in a more explicit form in Appendix B.

As the particle approaches the wall, the components of its mobility matrix, except for  $D_{\perp}^t$ , decrease to zero at contact due to hydrodynamic interactions. The coefficient  $D_{\perp}^t$  attains a finite value of

$$D_{\perp}^t(z=a) = D_0^t \frac{1}{\zeta(3)}, \quad (29)$$

with  $\zeta$  being the Riemann zeta function, for which  $1/\zeta(3) \approx 0.832$ . The dependence of the components of the mobility matrix on the wall-particle distance has been evaluated in numerous works, starting with approximate solutions from over a century ago by Lorentz<sup>43</sup> and Faxén,<sup>44</sup> followed by later calculations of Brenner *et al.*<sup>34,37,38,45</sup> and Dean and O'Neill.<sup>35,36</sup> These works, however, present only coarse approximations, valid for moderate wall-particle distances, and only for certain parts of the mobility matrix. More recently, full solutions in form of power series in inverse wall-particle distance  $t = a/z$ , have been obtained using high-precision numerical schemes based on the multipole method by Cichocki and Jones.<sup>29</sup> The latter work provides us with the most convenient form of these relations using the Padé approximants to incorporate both far-field effects and lubrication. Moreover, it contains all parts of the mobility matrix. We shall therefore use this representation for further calculations. For clarity, we introduce dimensionless mobility coefficients, rescaling them by the appropriate bulk values

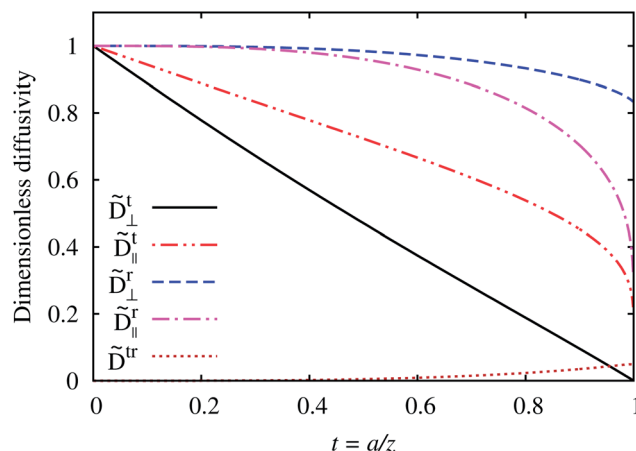


Fig. 2 The rescaled diffusion coefficients, defined in eqn (24)–(27) and (30), plotted as functions of dimensionless inverse distance from the wall  $t = a/z$ . As  $t \rightarrow 1$ , the diffusivities other than  $D_{\perp}^t$  vanish, becoming nonanalytic at  $t = 1$ . The effect of coupling, vanishing both at contact and far away from the wall, reaches its maximum of ca. 0.05 very close to the wall.

$$\tilde{D}_{\parallel,\perp}^t = \frac{D_{\parallel,\perp}^t}{D_0^t}, \tilde{D}_{\parallel,\perp}^r = \frac{D_{\parallel,\perp}^r}{D_0^r}, \tilde{D}^{\text{tr}} = \frac{D^{\text{tr}}}{aD_0^{\text{tr}}}. \quad (30)$$

We plot the dimensionless diffusion coefficients in Fig. 2 as functions of the inverse distance from the wall. It is worth noticing that the translational components of the diffusion matrix are more affected by hydrodynamic interactions than the rotational ones. The effect of translation–rotation coupling is usually small, although it becomes nonnegligible when the particle approaches the wall.

## 4 Short-time dynamics – derivation of the first cumulant

We start from a general expression for a time correlation function of two arbitrary phase-space functions  $f$  and  $g$ <sup>42</sup>

$$\langle f(t)g(0) \rangle = \int d\mathbf{X} f(\mathbf{X}) \exp\{\mathcal{L}t\} [g(\mathbf{X}) P^{\text{eq}}(\mathbf{X})], \quad (31)$$

where the equilibrium probability distribution  $P^{\text{eq}}$  is given by the wall–particle interaction potential  $\Phi(\mathbf{X})$  as  $P^{\text{eq}} \sim e^{-\beta\Phi(\mathbf{X})}$ , and  $\mathbf{X} = (\mathbf{r}, \hat{\mathbf{u}})$ , as defined before. Here we follow the notation and way of derivation outlined in earlier work of Cichocki *et al.*<sup>21</sup> We note that the electric field correlation function  $g_1(\mathbf{q}, t)$ , defined in eqn (2) is identical to eqn (31) with,

$$f(\mathbf{X}) = E_s(q; \mathbf{X}) = \mathcal{E}(\hat{\mathbf{u}}) \exp\{\mathbf{i}\mathbf{q} \cdot \mathbf{r}\} \exp\left\{-\frac{\kappa}{2}z\right\}, \quad (32)$$

$$g(\mathbf{X}) = f^*(\mathbf{X}), \quad (33)$$

in accordance with eqn (4).

Now, since we are interested in short-time dynamics, we approximate the exponential operator in eqn (31) to leading order in time

$$\exp\{\mathcal{L}t\} \approx 1 + \mathcal{L}t + \mathcal{O}(t^2). \quad (34)$$

The expressions for the first cumulant are most conveniently evaluated by noting that using eqn (17), and performing a partial integration, we may write

$$\int d\mathbf{X} f(\mathbf{X}) \mathcal{L}[g(\mathbf{X}) P^{\text{eq}}(\mathbf{X})] = - \int d\mathbf{X} P^{\text{eq}}(\mathbf{X}) [\nabla_{\mathcal{X}} f(\mathbf{X})] \cdot \mathbf{D} \cdot [\nabla_{\mathcal{X}} g(\mathbf{X})], \quad (35)$$

where the action of gradient operators is restricted to square brackets. Due to the particular structure of the diffusion tensor (22), the Smoluchowski operator can be decomposed into four parts

$$\mathcal{L} = \mathcal{L}^{\text{tt}} + \mathcal{L}^{\text{tr}} + \mathcal{L}^{\text{rt}} + \mathcal{L}^{\text{rr}}. \quad (36)$$

From now on, we will also drop the double index in tt and rr, simply writing t and r instead. With the help of (35), we can write the four contributions to the first cumulant as

$$\Gamma^t = \langle \nabla E_s \cdot \mathbf{D}^{\text{tt}} \cdot \nabla E_s^* \rangle / \langle |E_s|^2 \rangle, \quad (37)$$

$$\Gamma^r = \langle \mathbf{L} E_s \cdot \mathbf{D}^{\text{rr}} \cdot \mathbf{L} E_s^* \rangle / \langle |E_s|^2 \rangle, \quad (38)$$

$$\Gamma^{\text{tr}} = \langle \nabla E_s \cdot \mathbf{D}^{\text{tr}} \cdot \mathbf{L} E_s^* \rangle / \langle |E_s|^2 \rangle, \quad (39)$$

$$\Gamma^{\text{rt}} = \langle \mathbf{L} E_s \cdot \mathbf{D}^{\text{rt}} \cdot \nabla E_s^* \rangle / \langle |E_s|^2 \rangle, \quad (40)$$

where the averages are taken with respect to the equilibrium probability distribution  $P^{\text{eq}}$ . For brevity, we dropped the arguments of  $E_s$  and denoted  $\nabla = \frac{\partial}{\partial \mathbf{r}}$ . From the symmetry of the diffusion tensors (28) and the fact they depend solely on the distance to the particle from the wall and not on its orientation, it follows in a straightforward calculation that

$$\Gamma^{\text{tr}} + \Gamma^{\text{rt}} = 0, \quad (41)$$

in both VH- and VV-geometry. The proof of this fact can be found in Appendix A. The first cumulant simplifies then to

$$\Gamma = \Gamma^t + \Gamma^r, \quad (42)$$

and one may write explicit expressions for the translational and rotational parts

$$\Gamma^t = - \left\langle \left( \mathbf{i}\mathbf{q} - \frac{\kappa}{2} \hat{\mathbf{k}} \right) \cdot \mathbf{D}^{\text{tt}} \cdot \left( \mathbf{i}\mathbf{q} + \frac{\kappa}{2} \hat{\mathbf{k}} \right) \right\rangle_{\kappa}, \quad (43)$$

$$\Gamma^r = \frac{\left\langle \int d\hat{\mathbf{u}} [\mathbf{L}\mathcal{E}(\hat{\mathbf{u}})] \cdot \mathbf{D}^{\text{rr}} \cdot [\mathbf{L}\mathcal{E}^*(\hat{\mathbf{u}})] \right\rangle_{\kappa}}{\int d\hat{\mathbf{u}} |\mathcal{E}(\hat{\mathbf{u}})|^2}, \quad (44)$$

where the exponentially weighted ‘ $\kappa$ -average’ is defined as

$$\langle A \rangle_{\kappa} = \frac{\int_a^{\infty} dz e^{-\kappa(z-a)} e^{-\beta\Phi(z)} A(z)}{\int_a^{\infty} dz e^{-\kappa(z-a)} e^{-\beta\Phi(z)}}. \quad (45)$$

The rotational operator acting on the oriented dielectric tensor may be explicitly written as

$$\mathbf{L}\mathcal{E}(\hat{\mathbf{u}}) = \mathbf{L}(\hat{\mathbf{n}}_s \cdot \boldsymbol{\varepsilon}(\hat{\mathbf{u}}) \cdot \hat{\mathbf{n}}_0) = \Delta\alpha [(\hat{\mathbf{n}}_s \cdot \hat{\mathbf{u}}) \hat{\mathbf{u}} \times \hat{\mathbf{n}}_0 + (\hat{\mathbf{n}}_0 \cdot \hat{\mathbf{u}}) \hat{\mathbf{u}} \times \hat{\mathbf{n}}_s]. \quad (46)$$

We shall now decompose the scattering vector  $\mathbf{q}$  into its components parallel and perpendicular to the wall

$$\mathbf{q} = q_{\perp} \hat{\mathbf{k}} + \mathbf{q}_{\parallel}. \quad (47)$$

Evaluating eqn (43) and (44), we find the well-known expression for the translational contribution<sup>27</sup>

$$\Gamma^t = \langle D_{\parallel}^t \rangle_{\kappa} q_{\parallel}^2 + \langle D_{\perp}^t \rangle_{\kappa} \left( q_{\perp}^2 + \frac{\kappa^2}{4} \right), \quad (48)$$

which is independent of the scattering geometry. The expressions for the rotational contribution, depending on the VV or VH alignment of the experimental setup read<sup>28</sup>

$$\Gamma_{\text{VH}}^r = \langle D_{\parallel}^r \rangle_{\kappa} (2 + 3n_z^2) + \langle D_{\perp}^r \rangle_{\kappa} (1 + 3n_y^2), \quad (49)$$

$$\Gamma_{\text{VV}}^r = \frac{12|\Delta\alpha|^2}{45|\alpha|^2 + 4|\Delta\alpha|^2} \left( \langle D_{\parallel}^r \rangle_{\kappa} + \langle D_{\perp}^r \rangle_{\kappa} \right). \quad (50)$$

Interestingly, in the VH geometry, due to normalisation of  $g_1$  so that  $g_1(0) = 1$ , the rotational component is independent of the optical properties of the particle. In the VV geometry, the pre-factor depends on the characteristic polarisability properties of the material.

The expressions (48)–(50) are valid for an arbitrary potential of direct sphere–wall interactions. We will now restrict to hard–core interactions, so that  $\Phi = +\infty$  when there is overlap between the sphere and the wall, and  $\Phi = 0$  otherwise. Then, the average (45) reduces to

$$\langle A \rangle_\kappa = \kappa \int_a^\infty dz e^{-\kappa(z-a)} A(z). \quad (51)$$

To provide a fast predictive tool, we have tabulated the  $\kappa$ -averaged diffusion coefficients in Table 1. This allows for a convenient evaluation of theoretical predictions for the initial decay rate of  $g_1(\mathbf{q}, t)$ , without the need to use expensive computer simulations. For the numerical integration of diffusion coefficients, we have used the expressions for the hydrodynamic interaction functions by Cichocki and Jones.<sup>29</sup> The values of the cumulants can now be reproduced from eqn (48)–(50) by using the averaged values of the diffusion coefficients from Table 1.

It is worth noticing that for small penetration depths (corresponding to large values of  $\kappa a$ ), the averaged diffusion coefficients tend to their contact values at  $z = 0$ . It can be understood, as in this regime only the near-wall region is

**Table 1** Components of first cumulant approximation to  $g_1(\mathbf{q}, t)$  for hard–core interactions between the wall and the particle obtained by numerical integration of distance-dependent diffusivities of the particle near a wall. The coefficients are given here in the dimensionless form, in accord with eqn (30)

$\kappa a$	Translational coefficients		Rotational coefficients	
	$\langle \tilde{D}_{\parallel}^f \rangle_\kappa$	$\langle \tilde{D}_{\perp}^f \rangle_\kappa$	$\langle \tilde{D}_{\parallel}^r \rangle_\kappa$	$\langle \tilde{D}_{\perp}^r \rangle_\kappa$
0.1	0.884	0.781	0.983	0.994
0.2	0.831	0.682	0.968	0.989
0.3	0.791	0.612	0.954	0.983
0.4	0.761	0.559	0.942	0.979
0.5	0.736	0.516	0.931	0.976
0.6	0.715	0.481	0.920	0.971
0.7	0.697	0.451	0.910	0.968
0.8	0.681	0.425	0.901	0.965
0.9	0.667	0.403	0.892	0.962
1	0.654	0.383	0.884	0.960
1.1	0.643	0.365	0.876	0.957
1.2	0.632	0.349	0.868	0.955
1.3	0.622	0.335	0.861	0.952
1.4	0.614	0.322	0.854	0.949
1.5	0.605	0.310	0.848	0.947
1.7	0.591	0.288	0.836	0.944
1.9	0.578	0.270	0.825	0.940
2	0.572	0.262	0.820	0.939
5	0.473	0.140	0.716	0.907
7	0.442	0.108	0.677	0.896
9	0.420	0.088	0.647	0.888

illuminated and only particles in the proximity of the boundary contribute to the measured correlation function, and in consequence the hindrance effects of the wall are more pronounced. In general, the scaled values of averaged rotational diffusion coefficients are larger than the translational ones due to a much weaker dependence of  $D^{\text{tr}}$  on the distance from the wall, compared to the tt part, as presented in Fig. 2.

In the limit  $\kappa \rightarrow 0$ , corresponding to an infinite penetration depth, all of the above described quantities should converge towards their bulk DLS analogues. Indeed, our final results, eqn (48)–(50), reduce to well-known expressions from bulk scattering, given in eqn (11)–(13).

## 5 Beyond the first cumulant – numerical predictions

The decay of  $g_1(\mathbf{q}, t)$  for longer times, when the approximation by the first cumulant fails, is less understood, since there seems to be no exact expression for the decay rate. The relaxation of the correlation functions in EWDLS beyond the first cumulant may be studied by means of higher cumulants. This, however, may not always be possible due to their divergence. The higher cumulants contain higher-order derivatives of the diffusion coefficients, integrals of which are divergent due to the nonanalytic behaviour of those derivatives at contact with the wall, resulting from lubrication. We have discussed this matter in more detail in our earlier work.<sup>27</sup> To infer knowledge about the longer-time decay of  $g_1$ , we have therefore decided to employ a numerical Brownian dynamics scheme.

In our numerical simulations, we calculate the electric field correlation function  $g_1(\mathbf{q}, t)$  by averaging the expression (2) over many trajectories of a Brownian particle in its configuration space  $\mathbf{X} = (\mathbf{r}, \hat{\mathbf{u}})$ . We typically generated  $N = 10^5$  trajectories to obtain a statistical error of the order of 1%. The starting points are distributed initially according to an exponential weight  $e^{-\kappa z/2}$ . The statistics are then improved by exploiting the Markov property of diffusion processes, which allows multiple use of the same trajectories with different moments of time taken as starting points.<sup>46</sup>

The Brownian dynamics technique<sup>47</sup> relies on numerical integration of the Langevin equation, corresponding to the relevant Smoluchowski equation.<sup>48,49</sup> Explicit expressions for the Brownian dynamics increments to position and orientation, given in general by Dickinson *et al.*,<sup>50</sup> are discussed for a sphere in the presence of a wall in the work of Jones and Alavi.<sup>51</sup> Details of the algorithm are given in Appendix B. The length scale in the problem is set by the particle radius  $a$ , while the time scale is related to the structural relaxation time  $\tau = a^2/D_0^f$ , *i.e.* time needed by the particle to diffuse over a distance of its own radius.

Comparison of the approximation by the first cumulant and BD simulation is presented in Fig. 3. Due to the presence of an additional relaxation mode,  $I^{\text{tr}}$ , the decay of  $g_1$  is generally faster than compared to isotropic spherical particles exhibiting only translational motion. This effect is, however, much more

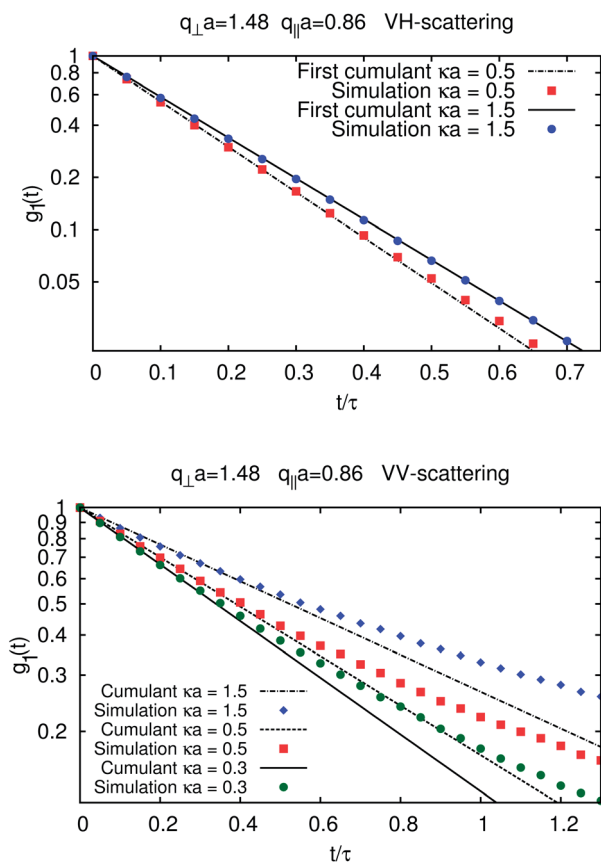


Fig. 3 Comparison of approximation by the first cumulant (9) and the BD simulation. Here, we assumed  $|\alpha| = |\Delta\alpha| = 1$  and  $n_y = n_z = 1/\sqrt{2}$  in VH mode. In both cases the decay may be accurately described by the first cumulant even for moderate times – up to 0.5 of the initial value of  $g_1$  for VV, and even for longer times for VH-geometry. The decay is generally faster in the VH case, as the additional rotational relaxation mode is more pronounced. The statistical error of simulation data is of the order of point size.

pronounced for VH-scattering, since the rotational contribution is independent of the dielectric properties of the particle.

## 6 Experimental details

### 6.1 Samples and Instrumentation

Experiments were performed on optically anisotropic spheres (Ausimont) made of a copolymer of tetrafluoroethylene (TFE) suspended in an aqueous NaCl-solution, with a salt concentration of  $10 \text{ mmol l}^{-1}$ , corresponding to a Debye screening length of 3 nm. This is sufficiently small to allow approximation of the interactions between the colloids and the wall by a hard core potential. The particles were dialysed extensively against  $10^{-2} \text{ mol l}^{-1}$  NaCl solution to ensure that all surfactants from the emulsion polymerisation were removed and therefore no steric stabilisation layers are present. The refractive index and the viscosity of the solvent were approximated by the values for water, that is  $n_2 = 1.33$  and  $\eta = 1 \text{ mPa s}$  at  $T = 293 \text{ K}$ . The radius of the particles was determined by bulk depolarized dynamic light scattering (DDLS) measurements to be  $a = 112 \text{ nm}$  with a

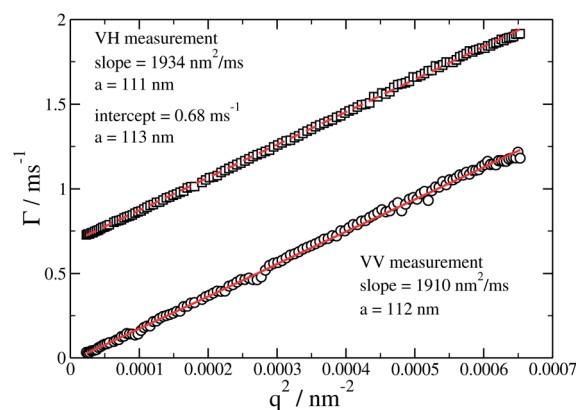


Fig. 4 The first cumulant  $\Gamma$  measured as a function of  $q^2$  in bulk DDLS experiments in VV and VH geometry. From the slopes of the dependencies, and the intercept of the VH curve, in accord with eqn (11)–(13), one may calculate the hydrodynamic radius of particles from the relevant diffusion coefficients (14), which confirms the spherical shape of the particles.

polydispersity of less than 10 percent, as indicated in Fig. 4. The fact that rotational and translational diffusion coefficients yield the same hydrodynamic radius when introduced into eqn (14) prove that the particles are of spherical shape.

In EWDLS experiments, laser light of vacuum wavelength  $\lambda_0$ , incident on the glass wall of the container filled with suspension at a great angle  $\alpha_i$  larger than the critical angle of total reflection, undergoes total internal reflection resulting in an evanescent wave entering the sample. The electric field strength of this wave decreases with the distance  $z$  from the wall as  $\exp(-\kappa z/2)$ , where the penetration depth  $2/\kappa$  is given by

$$\frac{2}{\kappa} = \lambda_0 / 2\pi \sqrt{(n_1 \sin \alpha_i)^2 - n_2^2}, \quad (52)$$

with  $n_1, n_2$  being the refractive indices of glass and solvent, respectively. By varying the incident angle, the penetration depth can be tuned, typically in the range of 100–800 nm. The scattering vector  $\mathbf{q} = \mathbf{k}_s - \mathbf{k}_i$  is the difference between the evanescent and scattered light wave vectors,  $\mathbf{k}_i$  and  $\mathbf{k}_s$ . For the needs of this analysis we decompose it into the components  $q_{\parallel}, q_{\perp}$ , parallel and perpendicular to the wall, respectively, as defined in eqn (47). In the EWDLS setup constructed in Forschungszentrum Jülich (Germany), these components can be independently changed by varying the angles  $\alpha_r$  and  $\theta$ , where  $\alpha_r$  is the angle between the vector  $\mathbf{k}_s$  and the wall, and  $\theta$  is the angle between the projection of  $\mathbf{k}_s$  on the wall and  $\mathbf{k}_i$  (see Fig. 5). The angles and the components of  $\mathbf{q}$  are related by

$$q_{\parallel} = 2\pi n_2 \sqrt{1 + \cos^2 \alpha_r - 2 \cos \alpha_r \cos \theta} / \lambda_0, \quad (53)$$

$$q_{\perp} = 2\pi n_2 \sin \alpha_r / \lambda_0. \quad (54)$$

In the present study we decided not to make use of this feature, since also the polarization vector of the scattered light depends on the scattering angles by

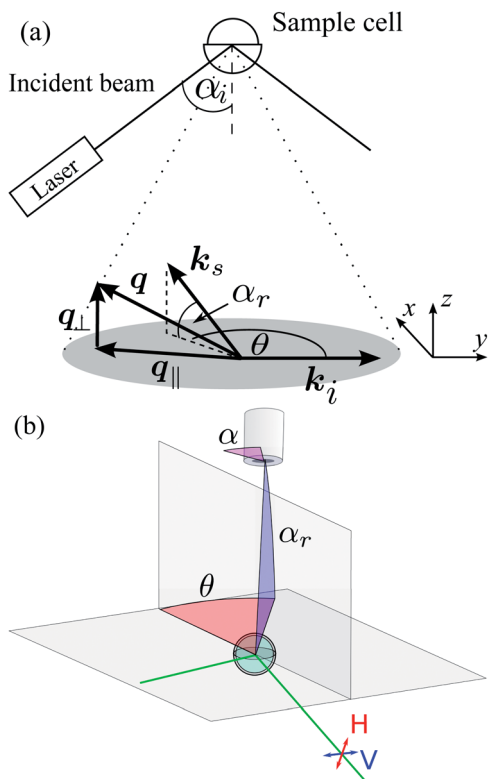


**Fig. 5** The geometry of EWDLS setup. (a) The illuminating light is the evanescent wave, which has the wave vector  $k_i$ , while the detector records light scattered in the direction of  $k_s$ . Note that here the  $x$ -direction is normal to the plane spanned by the primary and the totally reflected beam, while the  $z$ -direction is normal to the reflecting interface. (b) The angles  $\alpha_r$  and  $\theta$  define the scattering vector, while  $\alpha$  is the angle between the detector transmission direction and the plane, marked in blue, spanned by the wave vector of the scattered light and its projection onto the reflecting surface. The latter angle determines the scattering geometry (VH or VV).

$$\hat{n}_s = \begin{pmatrix} -\sin \alpha_r \sin \theta \cos \alpha + \cos \theta \sin \alpha \\ -\sin \alpha_r \cos \theta \cos \alpha - \sin \theta \sin \alpha \\ \cos \alpha_r \cos \alpha \end{pmatrix}, \quad (55)$$

with  $\alpha$  being the angle between the analyser transmission direction and the plane spanned by the wave vector of the scattered light and its projection onto the reflecting surface, as indicated in Fig. 5 (see also ref. 28). Therefore, it is rather cumbersome to maintain VV- or VH-geometry, while scanning only one of the scattering vector components. We rather choose to keep  $\theta = 0$  and scan only  $\alpha_r$  from 30 to 130 degree.

Hence, the decay rates of the measured correlation function depend on the penetration depth and two components of  $\mathbf{q}$ . Small values of  $\kappa^{-1}$  correspond to probing near-wall motion, while for larger values the results converge towards their bulk values. Relative magnitudes of the components of the scattering vector distinguish between measurements of diffusion along the wall (large  $q_{\parallel}$ ), or towards and away from the wall (large  $q_{\perp}$ ).

## 6.2 Data analysis

Compared to conventional DLS experiments, the analysis of correlation functions measured in EWDLS is usually hampered

by two problems. Firstly, there is always a static contribution to the scattered intensity, which originates from surface roughness and small impurities. This leads to a mixing of homodyne and heterodyne detection. To account for this, a general formulation of the Siegert relation has to be used to relate the field correlation function  $g_1(t)$  to the measured intensity correlation function  $g_2(t)$

$$g_2(t) = 1 + 2C_1 g_1(t) + (C_2 g_1(t))^2 \quad (56)$$

where  $C_2 = 1 - \sqrt{1 - A}$  and  $C_1 = C_2 - C_2^2$ , with  $A$  being the intercept of  $g_2(t)$ .<sup>26</sup> Secondly, EWDLS correlation functions often exhibit a very slow decay at large times. Although the physical origin of this slow relaxation has not been clarified yet, it was conjectured that the slow decay is due to inevitable stray-light originating from surface corrugations which is scattered into the detector by solute particles. The scattering vector of this contribution,  $\mathbf{q}_{\text{add}}$  would be roughly two orders of magnitude smaller than the regular scattering vectors for the given setup.<sup>27</sup> Accordingly, the scattered field which is detected contains an additional contribution with the phase  $\mathbf{q}_{\text{add}} \cdot \mathbf{r}(t)$ , and the corresponding correlation function will show an additional exponential relaxation at long times. Therefore we fit the long time part of the experimental TCF, typically at  $t > 10$  ms, by an exponential and subtract this contribution from the experimental data, which results a TCF which decays to  $g_2(t) - 1 = 0$  for large times. Subsequently the initial part ( $t < 0.2$  ms) of the resulting TCF is fitted with

$$g_2(t) = 1 + 2C_1 \exp\{-\Gamma t\} + (C_2 \exp\{-\Gamma t\})^2 \quad (57)$$

to determine the first cumulant,  $\Gamma$ .

## 7 Results

Examples for the initial part of typical correlation functions are shown in Fig. 6. There we compare experimental data obtained at different scattering geometries to theoretical first cumulant predictions, and simulations. The measured intensity TCFs were non-linear least squares fitted using the procedure described in Section 6.2, and the obtained parameter values were used to calculate the normalised field correlations functions,  $g_1(t)$ , shown in the plots. The simulation data, which were calculated free of adjustable parameters match the experimental data almost perfectly down to a correlation level of ten percent. Somewhat surprisingly, the first cumulant predictions agree very well with the experimental and the simulated data up to long times, which we demonstrate for a chosen set of data in Fig. 7. It is expected that the variation of the particles' diffusion coefficients along the  $z$ -direction, in combination with the evanescent illumination profile, causes a deviation of the TCF from a single exponential, similar to the deviation observed for TCFs obtained from samples with a large size polydispersity in bulk. However, if the penetration depth in an EWDLS experiment is small, as in the present case, the distribution of diffusion coefficients within the illuminated volume is small and consequently the correlation functions will deviate significantly from a single exponential only at large times.

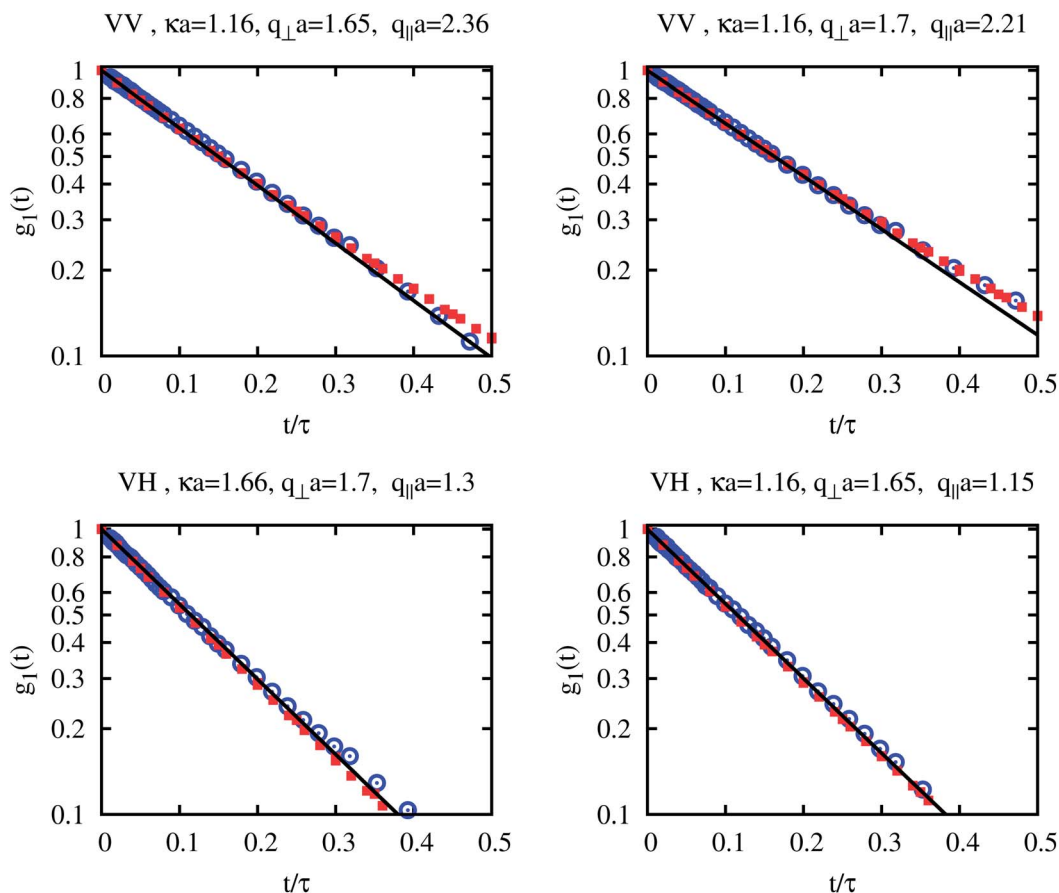


Fig. 6 Normalized electric field correlation functions  $g_1(t)$  recorded with different scattering geometries as indicated in the individual headlines. Blue circles are experimental data, red squares are simulation results and the full lines are theoretical first cumulant predictions, *i.e.*  $\exp(-\Gamma t)$ .

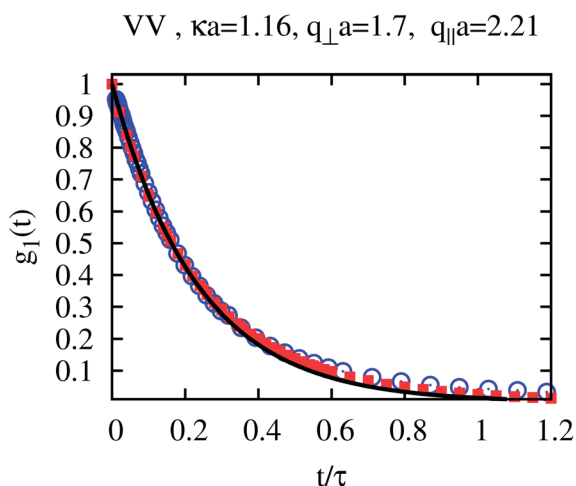


Fig. 7 Longer time decay of  $g_1$  – comparison of experimental data (blue circles), results of the BD simulations (red squares) and predictions by means of the first cumulant. Results are presented for a chosen set of parameters. The agreement is good even for moderate times.

The first cumulant values obtained from the data fitting are shown in Fig. 8. In the top part we plot  $\Gamma$  in dependence of the total scattering vector magnitude squared, while in the bottom

part the cumulants are plotted *versus*  $n_z^2$ . From both representations it is obvious that the parameter-free predictions for the first cumulant describe the experimental data correctly. Although the experimental data are scattered, it is obvious, that they follow the non linear variation with  $q_{\text{total}}^2$ , which is predicted by the theory. This non-linearity is due to the fact that  $q_{\text{total}} \approx q_{\perp}$  for low scattering angles, while at high angles  $q_{\parallel}$  is the dominating component. Accordingly, values of  $\Gamma$  are dominated by the diffusion normal to the interface at low  $q_{\text{total}}$  while at high  $q_{\text{total}}$  the diffusion parallel to the interface is prominent.

The expressions for the first cumulant in EWDLS (48)–(50) and DDLS (11)–(13) reflect an important distinguishing property – even for large optical anisotropy, the amplitude of the rotational contribution in the VV case is much smaller than in the VH case. From bulk SLS measurement we determine the ratio of averaged scattered intensities to be  $I_{\text{VH}}/I_{\text{VV}} \approx 1/20$ . Since<sup>41</sup>

$$\frac{I_{\text{VH}}}{I_{\text{VV}}} = \frac{|\Delta\alpha|^2}{15|\alpha|^2 + \frac{4}{3}|\Delta\alpha|^2}, \quad (58)$$

we may then use this ratio and eqn (49) and (50) to estimate the rotational contribution to  $\Gamma$  in the VV case to be of the order of 5% at  $(qa)^2 \approx 2$  and decreasing with increasing  $qa$ .

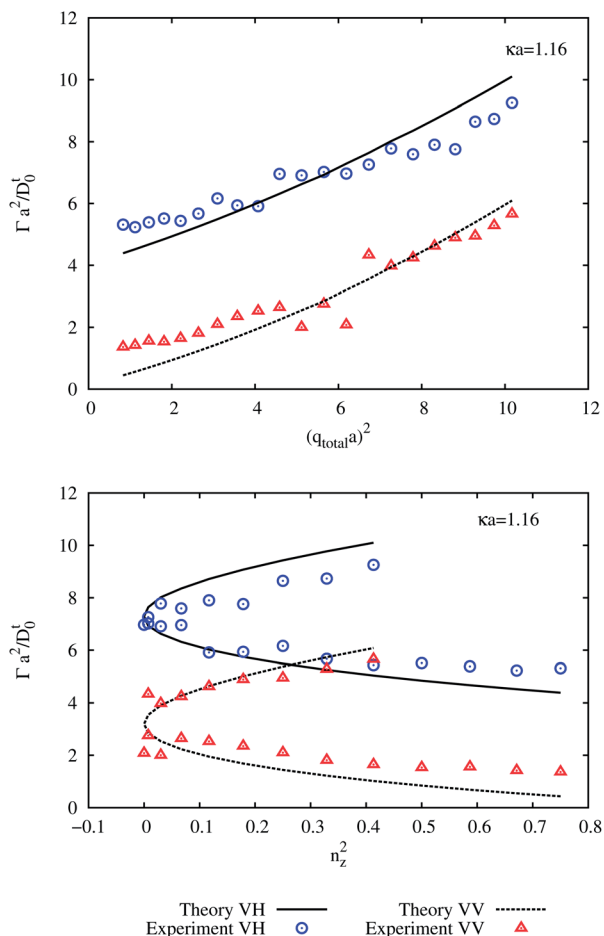


**Fig. 8** First cumulants vs. the total scattering vector squared (top) and vs. the z-component of the scattered light polarization vector squared (bottom). Symbols are experimental data obtained in VV (red triangles) and VH (blue circles) while the lines represent theoretical predictions for the first cumulant.

Therefore, as this ratio is not very large, we might approximate the first cumulant in VV-geometry not to have any rotational contribution. One can then measure the sole rotational component in the VH case, described by eqn (49), by measuring the full initial decay rate in VH and VV and subtracting one from the other

$$\Gamma_{\text{VH}}^r \approx \Gamma_{\text{VH}} - \Gamma_{\text{VV}}. \quad (59)$$

In this way, at the level of the first cumulant, translations and rotations may be decoupled and therefore purely rotational properties become experimentally accessible.<sup>28</sup>

The rotational contribution to the TCF relaxation,  $\Gamma_{\text{VH}}^r$  is plotted vs.  $n_z^2$  in Fig. 9. As these data represent the difference of two sets of experimental results, which each have a relative error of five to ten percent, the  $\Gamma_{\text{VH}}^r$  are rather scattered. Nevertheless, they show the linear trend predicted by eqn (49), which is added as a solid line to the graph. Since  $n_z^2 + n_y^2 = 1$ , eqn (49) may be reformulated as

$$\Gamma_{\text{VH}}^r = 2\langle D_{\parallel}^r \rangle_{\kappa} + 4\langle D_{\perp}^r \rangle_{\kappa} + 3(\langle D_{\parallel}^r \rangle_{\kappa} - \langle D_{\perp}^r \rangle_{\kappa})n_z^2 \quad (60)$$

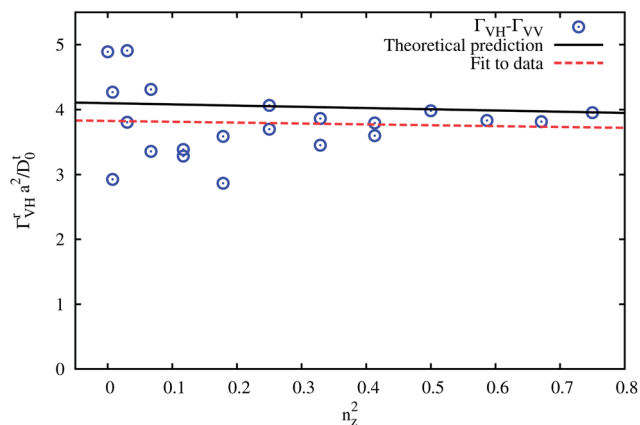


**Fig. 9** Rotational relaxation rate vs. the z-component of the scattered light polarization vector squared. The points represent the experimental data, as given by eqn (59), while the theoretical prediction linear in  $n_z^2$ , marked with the solid line, follows from eqn (60). A linear fit to data results in diffusion coefficients differing from theoretically predicted  $\langle D_{\parallel}^r \rangle_{\kappa}$  and  $\langle D_{\perp}^r \rangle_{\kappa}$  by 5% and 7.5%, respectively.

indicating that averaged rotational diffusion constants can be determined from the intercept and the slope of a linear regression of  $\Gamma_{\text{VH}}^r$  vs.  $n_z^2$ . In Fig. 9, a linear fit to data results in a fair agreement with theoretical predictions, with both diffusivities differing by less than 8% from the theoretical predictions.

## 8 Conclusions

In this article, we have presented a broad perspective on the theoretical framework, within which it is possible to derive exact expressions for the translational and rotational contributions to the first cumulant of the electric field correlation function, which can be measured in experiments on wall-bounded colloidal suspensions at low densities. We have demonstrated the importance of some inherent features of evanescent wave dynamic light scattering, including the effects of non-uniform illumination of the sample, and the hindrance of particles' diffusivities near a hard boundary. The averaged diffusion coefficients, which we have calculated and presented in a table for a wide range of penetration depths, constitute a practical tool for experimentalists, as it provides a convenient way to calculate the first cumulant, using the expressions given in the paper.

In order to investigate the quality of approximation by the first cumulant, and to go beyond its applicability, we have also developed a Brownian dynamics simulation, predictions of which have been found in good agreement with the first cumulant, as well as with the experimental data measured on a dilute suspension of optically anisotropic spherical colloids using an EWDLs setup in Jülich (Germany).

Finally, by removing the slow mode contribution from the experimental data to account for the effects of a nonzero baseline, we have found very good agreement between theoretical predictions and experimental results, free of adjustable parameters. This in turn gives us the possibility to extract the averaged diffusion coefficients, both translational and

rotational, and opens a new way of determining the effects of confinement on colloidal dynamics experimentally.

## Appendix A – vanishing of the tr and rt parts of the first cumulant

We shall now prove that the coupling contribution to the first cumulant vanishes,  $\Gamma^{\text{tr}} = \Gamma^{\text{rt}} = 0$ , independently of the scattering geometry, provided that the dielectric tensor of the particle has the form as in eqn (6). The starting point here is the expressions for those contributions given in eqn (39) and (40). In those expressions, due to the fact that the diffusion matrix and the interaction potential depend only on the position of the particle and not on its orientation, using the form of electric field as in eqn (5), one encounters angular averages involving the expression

$$\mathcal{E}(\hat{\mathbf{u}})L\mathcal{E}^*(\hat{\mathbf{u}}), \quad (61)$$

and its complex conjugate. According to eqn (6), the quantity  $\mathcal{E}(\hat{\mathbf{u}})$  contains an isotropic part proportional to  $\alpha$ , and an orientation-dependent contribution proportional to  $\Delta\alpha$ . Since  $L$  can be regarded as differentiation with respect to angles describing the orientation, we have

$$\int d\hat{\mathbf{u}}L(\dots) = 0, \quad (62)$$

for an arbitrary function of orientation. Using this property, we immediately conclude that the isotropic part of  $\mathcal{E}(\hat{\mathbf{u}})$ , producing in eqn (61) a term proportional to  $L\mathcal{E}^*(\hat{\mathbf{u}})$ , averages out to zero. Therefore only the anisotropic part contributes, resulting in an expression  $\Delta\alpha(\hat{\mathbf{n}}_s \cdot \hat{\mathbf{u}}\hat{\mathbf{u}} \cdot \hat{\mathbf{n}}_0)L\mathcal{E}^*(\hat{\mathbf{u}})$ . The rotational operator acting on  $\mathcal{E}(\hat{\mathbf{u}})$  acts also only on the nonisotropic part, as the orientation-independent term vanishes under the action of a derivative. The result of this operation is proportional to the complex polarisability anisotropy  $\Delta\alpha$ . Due to the structure of eqn (39) and (40), in both terms we arrive at real-valued expressions

$$|\Delta\alpha|^2(\hat{\mathbf{n}}_s \cdot \hat{\mathbf{u}}\hat{\mathbf{u}} \cdot \hat{\mathbf{n}}_0)L(\hat{\mathbf{n}}_s \cdot \hat{\mathbf{u}}\hat{\mathbf{u}} \cdot \hat{\mathbf{n}}_0) = \frac{1}{2}|\Delta\alpha|^2L(\hat{\mathbf{n}}_s \cdot \hat{\mathbf{u}}\hat{\mathbf{u}} \cdot \hat{\mathbf{n}}_0)^2, \quad (63)$$

which again average out to zero.

## Appendix B – Brownian dynamics algorithm for a sphere near a wall

The Langevin equation,<sup>48</sup> which lies at the root of Brownian dynamics simulations, is usually obtained from the corresponding Smoluchowski equation (eqn (16)). In case of a single hard-core particle in a wall-bounded fluid, we may use the structure of the diffusion matrix  $\mathbf{D}$ , given in eqn (24)–(28) to rewrite the Smoluchowski equation in a more explicit form

$$\frac{\partial P}{\partial t} = \frac{\partial}{\partial z} \left( D_{\perp}^{\text{t}}(z) \frac{\partial P}{\partial z} \right) + D_{\parallel}^{\text{t}}(z) \left( \frac{\partial^2}{\partial x^2} + \frac{\partial^2}{\partial y^2} \right) P + D_{\parallel}^{\text{r}}(z) L_z^2 P + D_{\perp}^{\text{r}}(z) [L^2 - L_z^2] P + 2D^{\text{tr}}(z) \cdot (\nabla \times \mathbf{L})_z P, \quad (64)$$

where the versor  $\hat{\mathbf{k}}$  indicates again the direction normal to the wall, and we have denoted  $A_z = \hat{\mathbf{k}} \cdot \mathbf{A}$  for any vector  $\mathbf{A}$ . The Euler integration scheme basing on a corresponding Langevin

equation was given earlier by Jones and Alavi.<sup>51</sup> Below, we briefly describe the update rules for the configuration  $\mathbf{X} = (\mathbf{r}, \hat{\mathbf{u}})$  of the particle in a short period of time  $\Delta t$ . We use the dimensionless units described in Section 5. In the following, we rescaled the diffusivities by their bulk values, as defined in eqn (30). Suppose the initial coordinates at the beginning of the step to be  $(\mathbf{r}_0, \hat{\mathbf{u}}_0)$  at time  $t_0$ . In a time step of  $\Delta t$  the coordinates attain their new values  $(\mathbf{r}, \hat{\mathbf{u}})$  in accordance with the following update rules

$$\mathbf{r} = \mathbf{r}_0 + \frac{d\tilde{D}_{\perp}^{\text{t}}}{dz} \hat{\mathbf{k}} \Delta t + \mathbf{s}^{\text{t}}, \quad (65)$$

$$\hat{\mathbf{u}} = \frac{\mathbf{u}'}{|\mathbf{u}'|}, \quad (66)$$

where

$$\mathbf{u}' = \hat{\mathbf{u}}_0 - \frac{3}{4} \left( \tilde{D}_{\perp}^{\text{r}} - \tilde{D}_{\parallel}^{\text{r}} \right) \left( u_{z,0}^2 \hat{\mathbf{u}}_0 - u_{z,0} \hat{\mathbf{k}} \right) \Delta t + \mathbf{s}^{\text{r}} \times \hat{\mathbf{u}}_0, \quad (67)$$

with  $u_{z,0} = \hat{\mathbf{k}} \cdot \hat{\mathbf{u}}_0$ . All the diffusivities on the right-hand side are evaluated at the initial position  $z_0$ . The random displacement vector  $\mathbf{S} = (a\mathbf{s}^{\text{t}}, \mathbf{s}^{\text{r}})$  has to satisfy the conditions

$$\langle \mathbf{S} \rangle = 0, \quad \langle \mathbf{S}\mathbf{S} \rangle = 2\Delta t \mathbf{D}, \quad (68)$$

where  $\mathbf{D}$  is the diffusion matrix for a sphere at  $(\mathbf{r}_0, \hat{\mathbf{u}}_0)$ . The explicit expressions for the noise term may be obtained by performing standard<sup>47</sup> Cholesky decomposition of the diffusion tensor  $D_{ij} = B_{ik}B_{jk}$  and generating six independent Gaussian random variables  $f_i$  having the stochastic properties

$$\langle f_i \rangle = 0, \quad \langle f_i f_j \rangle = 2\delta_{ij} \Delta t. \quad (69)$$

The indices  $i = 1, 2, 3$  refer to translational components along  $x, y, z$ , respectively, while  $i = 4, 5, 6$  describe the rotations along these axes. We may now write the required noise terms as

$$s_i = \sum_{j=1}^6 B_{ij} f_j, \quad (70)$$

where the components of  $\mathbf{B}$  are given by<sup>51,52</sup>

$$\begin{aligned} B_{11} = B_{22} &= \sqrt{\tilde{D}_{\parallel}^{\text{t}}}, \quad B_{33} = \sqrt{\tilde{D}_{\perp}^{\text{t}}}, \\ B_{42} = -B_{51} &= -\frac{3}{4} \frac{\tilde{D}^{\text{tr}}}{\sqrt{\tilde{D}_{\parallel}^{\text{t}}}}, \\ B_{44} = B_{55} &= \frac{3}{4} \frac{1}{\sqrt{\tilde{D}_{\parallel}^{\text{t}}}} \left( \frac{4}{3} \tilde{D}_{\parallel}^{\text{t}} \tilde{D}_{\parallel}^{\text{r}} - (\tilde{D}^{\text{tr}})^2 \right)^{1/2}, \\ B_{66} &= \frac{1}{2} \sqrt{3\tilde{D}_{\perp}^{\text{r}}}. \end{aligned} \quad (71)$$

We would like to emphasize that the routine presented here can be simplified by reducing the number of degrees of freedom, provided that we disregard the translational-rotational motion coupling. Indeed, letting  $D^{\text{tr}} = 0$  in eqn (64), we arrive at an equation describing rotational and translational diffusion with only coupling encoded in the  $z$ -dependence of the diffusion matrix. We may now proceed as follows – due to the translational

invariance of the system in the parallel ( $xy$ ) plane, we may perform a two-dimensional Fourier transform in these directions, thus eliminating  $x$  and  $y$  in favour of  $q_{\parallel}$ , which is a fixed parameter. Therefore, the description reduces to three independent variables ( $z, \hat{u}$ ) and eqn (64) reduces to a diffusion-reaction equation with a sink. For purely translational motion, this procedure has been described in detail in our earlier work.<sup>27</sup> These results can be easily generalised to include rotations. The simplified routine greatly reduces the time needed for simulations. In this article, however, we have decided to perform full BD simulation. The validity of the simplified scheme, with the neglect of tr coupling, still needs further investigation.

## Acknowledgements

Maciej Lisicki wishes to acknowledge support from the National Center of Science grant no. 2012/07/N/ST3/03120. This work was supported by the Foundation for Polish Science International PhD Projects Programme co-financed by the EU European Regional Development Fund. The authors acknowledge financial support from the EU through FP7, project Nanodirect (Grant no. NMP4-SL-2008-213948) and from the European Commission under the Seventh Framework Program by means of the grant agreement for the Integrated Infrastructure Initiative N. 262348 European Soft Matter Infrastructure (ESMI).

## References

- Z. Cheng and T. G. Mason, *Phys. Rev. Lett.*, 2003, **90**, 018304.
- R. Cherry, A. Bürkli, M. Busslinger and G. Schneider, *Nature*, 1976, **263**, 389.
- R. A. Cone, *Nat. New Biol.*, 1972, **236**, 39.
- R. Carlson, C. Gabel, S. Chan and R. Austin, *Biomed. Microdevices*, 1998, **1**, 39–47.
- M. Eigen and G. G. Hammes, *Advances in Enzymology and Related Subjects of Biochemistry*, ed. F. F. Ford, John Wiley & Sons, Hoboken, NJ, 1963, vol. 25, p. 1.
- K. Solc and W. H. Stockmayer, *J. Chem. Phys.*, 1971, **54**, 2981.
- R. J. Hall and D. A. Greenhalgh, *Opt. Commun.*, 1982, **40**, 417–420.
- T. Squires and S. Quake, *Rev. Mod. Phys.*, 2005, **77**, 977.
- C. Rice and R. Whitehead, *J. Phys. Chem.*, 1965, **69**, 4017.
- D. Psaltis, S. R. Quake and C. Yang, *Nature*, 2006, **442**, 381.
- T. Sawetzki, S. Rahmouni, C. Bechinger and D. W. M. Marr, *Proc. Natl. Acad. Sci. U. S. A.*, 2008, **105**, 20141.
- E. Lauga and T. R. Powers, *Rep. Prog. Phys.*, 2009, **72**, 096601.
- I. H. Riedel, K. Kruse and J. Howard, *Science*, 2005, **309**, 300.
- C. Effenhauser, G. Bruin and A. Paulus, *Electrophoresis*, 1997, **18**, 2203.
- K. H. Lan, N. Ostrowsky and D. Sornette, *Phys. Rev. Lett.*, 1986, **57**, 17.
- N. Garnier and N. Ostrowsky, *J. Phys. II France*, 1991, **1**, 1221.
- M. I. M. Feitosa and O. N. Mesquita, *Phys. Rev. A: At., Mol., Opt. Phys.*, 1991, **44**, 6677.
- H. Matsuoka, H. Morikawa, S. Tanimoto, A. Kubota, Y. Naito and H. Yamaoka, *Colloid Polym. Sci.*, 1998, **276**, 349.
- V. N. Michailidou, G. Petekidis, J. W. Swan and J. F. Brady, *Phys. Rev. Lett.*, 2009, **102**, 068302.
- V. N. Michailidou, J. W. Swan, J. F. Brady and G. Petekidis, *J. Chem. Phys.*, 2013, **139**, 164905.
- B. Cichocki, E. Wajnryb, J. Bławdziewicz, J. K. G. Dhont and P. R. Lang, *J. Chem. Phys.*, 2010, **132**, 074704.
- B. Loppinet, G. Petekidis and G. Fytas, *Langmuir*, 1998, **14**, 4958.
- G. Fytas, S. H. Anastasiadis, R. Seghrouchni, D. Vlassopoulos, J. Li, B. J. Factor, W. Theobald and C. Toprakcioglu, *Science*, 1998, **274**, 2041.
- G. E. Yakubov, B. Loppinet, H. Zhang, J. Rhe, R. Sigel and G. Fytas, *Phys. Rev. Lett.*, 2004, **92**, 115501.
- P. Holmqvist, J. K. G. Dhont and P. R. Lang, *Phys. Rev. E: Stat., Nonlinear, Soft Matter Phys.*, 2006, **74**, 021402.
- P. Holmqvist, J. K. G. Dhont and P. R. Lang, *J. Chem. Phys.*, 2007, **126**, 044707.
- M. Lisicki, B. Cichocki, J. K. G. Dhont and P. R. Lang, *J. Chem. Phys.*, 2012, **136**, 204704.
- S. A. Rogers, M. Lisicki, B. Cichocki, J. K. G. Dhont and P. R. Lang, *Phys. Rev. Lett.*, 2012, **109**, 098305.
- B. Cichocki and R. B. Jones, *Physica A*, 1998, **258**, 273.
- R. B. Jones, *Physica A*, 1988, **150**, 339.
- V. Degiorgio, R. Piazza and T. Bellini, *Adv. Colloid Interface Sci.*, 1994, **48**, 61.
- R. Piazza, V. Degiorgio, M. Corti and J. Stavans, *Phys. Rev. B: Condens. Matter Mater. Phys.*, 1990, **42**, 4885.
- V. Degiorgio, R. Piazza and R. B. Jones, *Phys. Rev. E: Stat. Phys., Plasmas, Fluids, Relat. Interdiscip. Top.*, 1995, **52**, 2707.
- H. Brenner, *Chem. Eng. Sci.*, 1961, **16**, 242.
- W. Dean and M. O'Neill, *Mathematika*, 1963, **10**, 13.
- W. Dean and M. O'Neill, *Mathematika*, 1964, **11**, 67.
- A. Goldman, R. Cox and H. Brenner, *Chem. Eng. Sci.*, 1967, **22**, 637.
- A. Goldman, R. Cox and H. Brenner, *Chem. Eng. Sci.*, 1967, **22**, 653.
- R. B. Jones, *J. Chem. Phys.*, 2005, **123**, 164705.
- R. Sigel, *Curr. Opin. Colloid Interface Sci.*, 2009, **14**, 426–437.
- B. J. Berne and R. Pecora, *Dynamic Light Scattering: With Applications to Chemistry, Biology, and Physics*, Dover Publications, 2000.
- J. K. G. Dhont, *An Introduction to Dynamics of Colloids*, Elsevier, 1996.
- H. A. Lorentz, *Abhandlung über Theoretische Physik*, ed B. G. Teubner, Leipzig und Berlin, 1907.
- H. Faxén, *Ark. Mat., Astron. Fys.*, 1923, **17**, 1.
- J. Happel and H. Brenner, *Low Reynolds Numbers Hydrodynamics*, Kluwer, Dordrecht, 1991.
- D. Frenkel and B. Smit, *Understanding Molecular Simulation: From Algorithms to Applications*, Elsevier Science, 2001.
- D. L. Ermak and J. A. McCammon, *J. Chem. Phys.*, 1978, **69**, 1352–1360.
- N. G. Van Kampen, *Stochastic Processes in Physics and Chemistry*, 3rd edn, Elsevier, North Holland, 2007.
- T. J. Murphy and J. Aguirre, *J. Chem. Phys.*, 1972, **57**, 2098.
- E. Dickinson, S. A. Allison and J. A. McCammon, *J. Chem. Soc., Faraday Trans. 2*, 1985, **81**, 591.
- R. B. Jones and F. N. Alavi, *Physica A*, 1992, **187**, 436.
- C. B. Korn and U. S. Schwarz, *J. Chem. Phys.*, 2007, **126**, 095103.